Applied Surface Science 720 (2026) 165243

Contents lists available at ScienceDirect

Applied Surface Science

journal homepage: www.elsevier.com/locate/apsusc

Full Length Article

A clean photochemical pathway for reconfiguring the sporopollenin biopolymer into sustainable interfaces for biocompatible cellular applications

Volkan Aylanc [a,b,c,**], Andreia F. Peixoto [b], Ricardo C. Calhelha [a], Olívia S.G.P. Soares [d,e], Nuno Vale [c,f], Cristina Freire [b], Miguel Vilas-Boas [a,*]

[a] CIMO, LA SusTEC, Instituto Politécnico de Bragança, Campus de Santa Apolónia, 5300-253 Bragança, Portugal
[b] LAQV-REQUIMTE-, Departamento de Química e Bioquímica, Faculdade de Ciências, Universidade do Porto 4169-007, Porto, Portugal
[c] PerMed Research Group, Center for Health Technology and Services Research (CINTESIS), 4200-450 Porto, Portugal
[d] ALiCE – Associate Laboratory in Chemical Engineering, Faculty of Engineering, University of Porto 4200-465, Porto, Portugal
[e] LSRE-LCM - Laboratory of Separation and Reaction Engineering - Laboratory of Catalysis and Materials Faculty of Engineering, University of Porto 4200-465, Porto, Portugal
[f] Department of Community Medicine, Health Information and Decision (MEDCIDS), Faculty of Medicine, University of Porto 4200-319 Porto, Portugal

ARTICLE INFO

Keywords:
Biointerface engineering
Natural microcapsules
UV-C irradiation
Surface functionalization
Cancer cell adhesion

ABSTRACT

Sporopollenin material, derived from pollen grains, provides a natural and sustainable platform for applications in advanced materials, controlled drug delivery, and surface engineering due to its exceptional structural robustness and chemical stability. However, its inert surface chemistry limits biological interactions, requiring controlled surface modification to enhance biointerface performance. This study presents a clean photochemical strategy for reconfiguring the surface of sporopollenin biopolymer, thereby improving its biocompatibility and cellular adhesion. Seven sporopollenin microcapsules (SMCs) of varying sizes (12.5–36.3 μm), purified from bee pollen pellets, were exposed to ultraviolet-C (UV-C) irradiation. Characterization by water contact angle, atomic force microscopy (AFM), Fourier-transform infrared spectroscopy (FTIR), and X-ray photoelectron spectroscopy (XPS) revealed pronounced surface oxidation (O/C ratio increase of up to 78 %) and enrichment in polar functional groups (hydroxyl, carbonyl, and carboxyl), without compromising structural integrity. These modifications induced superhydrophilicity and enhanced cell interaction. Biocompatibility testing using Vero normal cells confirmed SMCs' safety (GI_{50} > 700 μg/mL), while 2,2-diphenyl-1-picrylhydrazyl ($DPPH^{\bullet}$) assays indicated higher radical scavenging activity, correlating with surface functionalization. Notably, treated SMCs exhibited up to 52 % higher binding to colorectal cancer cells, Caco-2, as confirmed by scanning electron microscope (SEM) and confocal laser scanning microscopy (CLSM). Overall, this clean photochemical route effectively enhances the interface potential of natural sporopollenin biopolymer for future drug delivery, regenerative medicine, and tissue engineering applications.

1. Introduction

Microcapsule structures, whether naturally occurring or engineered from processable resources, have gained considerable interest across various research fields [1,2]. These include pharmaceuticals [3], where they are used for drug encapsulation and controlled release at specific sites; the food industry [4], where they aid in preserving, distributing, and stabilizing bioactive compounds and probiotics; separation technology [2,5], which assists in removing heavy metals and environmental contaminants; and diagnostics [6], where they are utilized in sensors and medical imaging. Among the diverse types of microcapsules explored, bio-based systems have attracted particular attention due to their sustainability and compatibility with biological applications.

The value of bio-based microcapsules for sustainability and bio-

* Corresponding author at: LAQV-REQUIMTE-, Departamento de Química e Bioquímica, Faculdade de Ciências, Universidade do Porto, 4169-007, Porto, Portugal.
** Corresponding author at: Centro de Investigação de Montanha (CIMO), Instituto Politécnico de Bragança, Campus de Santa Apolónia, 5300-253 Bragança, Portugal.
E-mail addresses: volkanaylanc@yahoo.com (V. Aylanc), mvboas@ipb.pt (M. Vilas-Boas).

https://doi.org/10.1016/j.apsusc.2025.165243
Received 15 October 2025; Received in revised form 10 November 2025; Accepted 11 November 2025
Available online 12 November 2025

related applications lies in the abundant availability of biomaterials, often sourced from nature or even as biomass residues [7]. The extensive range of possible processing approaches, coupled with the versatility of their chemical composition, positions these materials as an obvious and advantageous choice [3,8]. While the specific characteristics of ideal bio-based microcapsules vary according to the intended application, certain fundamental requirements should be met, especially for practices involving biological systems [9]. These requirements include biocompatibility, signifying the material's ability to elicit an appropriate host response in a given application; biomechanical stability, ensuring resilience against various mechanical stresses during processing and application; bioactivity, referring to the capacity to form a chemical or physiological bond with body tissues; green processing, avoiding harsh organic solvents throughout processing, production, and functionalization steps; and a commitment to using environmentally safe and sustainable raw materials for commercial viability [10–12]. In efforts to design materials that satisfy these criteria, several biological origin polymers have been explored as promising building blocks for microcapsule fabrication.

Microcapsules derived from amino acid chains (e.g., collagen, elastin), sugar chains (e.g., alginate, cellulose), and nucleotide chains (DNA, RNA) possess the potential to meet all or most of the aforementioned requirements [13,14]. However, the construction of such microcapsules may involve a protracted and intricate process, requiring sophisticated equipment. Furthermore, the resultant products may lack uniform size distribution and long-term mechanical stability [15]. To address these challenges, pollen grains, serving as natural microcapsules, have emerged as promising candidates. Pollen-based microcarriers, originally designed by nature for the transport of plant reproductive material, boast well-adapted molecular wall designs developed over millions of years of evolution [3]. The pollen grain wall comprises two fundamental layers: the outer wall (exine), composed of sporopollenin, a highly cross-linked biopolymer featuring aliphatic chains linked to aromatic moieties, conjugated phenols, and aliphatic alcohols, and the inner wall (intine), composed of cellulose and pectin [2,16].

SMCs exhibit an array of functional properties, including mechanical robustness, biocompatibility, chemical inertness, a spacious internal cavity, species-specific size monodispersity, unique surface architecture, and nanochannels along with apertures, making them excellent platforms for loading and releasing functional therapeutics [2,3,15,16]. Notably, the production of SMCs does not require complex methodologies or devices to achieve desired morphological features, and their purification can be accomplished through a simple chemical method [16,17]. Using sustainable biomasses such as bee pollen pellets or direct plant pollen as raw sources enhances the eco-friendliness of SMCs. Herein, we opted for bee pollen pellets as a raw source, drawn by several potential advantages. For example, each bee pollen pellet (with an average diameter of 3–5 mm and a weight of 15 mg (fresh) comprises pollen grains originating from a single plant species, ensuring a uniform source [3,18]. The availability of these pellets from a single point, typically a hive or apiary, facilitates rapid and convenient collection [19,20]. Further, bee pollen has been recognized throughout history as a valuable food and remedy, and today, it is commercially available in markets either in its raw form or as a significant component of functional foods, thanks to its high protein and carbohydrate content and associated health benefits [21].

Despite the numerous opportunities presented by SMCs in bulk, there is a need for modifications to extend their utility beyond specific applications. A key aspect requiring attention is the surface characteristics, as SMCs predominantly exhibit hydrophobic behavior [8,9], a characteristic that can limit their application versatility. Considering that a significant number of biological reactions take place at surfaces and interfaces, factors such as the chemical structure of the material, surface topography, roughness, and hydrophilicity play crucial roles in determining compatibility with host cells [12,22].

Even though numerous studies described the optimization of the surface and chemical properties of SMCs in environmental remediation applications [2,23,24], the exploration of their potential cellular tailoring is rather limited. To enhance surface wettability and consequently cellular adhesion, Tan et al. [8] demonstrated that UV-ozone treatment of natural pollen grains from *Camellia sinensis* increased the surface elemental oxygen and ketone ratio, resulting in improved particle dispersibility and enhanced cellular adhesion. Another study [16] noted that SMCs from *Lycopodium clavatum* increased hydrophilicity through a reduction in phosphoric acid treatment temperature from 160 °C to 60 °C, following acetone and potassium hydroxide treatment during purification. Similar findings were reported by Li et al. [25] for pine SMCs, achieved through sodium hydroxide treatment at 80 °C after the phosphoric acid step. However, these studies fall short of providing specific cellular applications for surface-modified microcapsules, leaving a gap in understanding the mechanisms and potential interactions between SMCs and cells/biological tissues. Another way of exploration in surface modification involves coating with biopolymers. Zhou et al. [9] showed that coating *Helianthus annuus* SMCs with poly-L-lysine hydrobromide and poly-L-glutamic acid sodium salt, using the layer-by-layer technique, increased wetting and improved particle/cell adhesion. It is crucial to acknowledge, however, that coating techniques may come with a drawback, long-term instability of the created layer and observed delamination due to a mismatch between the mechanical properties of the biopolymer substrate and the created layer [11].

Hence, physical surface modification applications present a viable alternative. Herein, we introduced UV-C irradiation, for the first time, to modify the surfaces of SMCs exhibiting various morphological characteristics sourced from bee pollen pellets. UV-C irradiation, as an alternative to harsh chemicals, has previously been explored for modifying the surfaces of certain biopolymeric and synthetic-based materials [22,26–28]. A distinctive feature of this method is its selectivity, targeting only the top surface of microcapsules [11]. Furthermore, UV-C irradiation thus emerges as a robust and sustainable functionalization strategy due to its solvent-free operation, energy efficiency, and absence of chemical initiators [11,27]. Consequently, a majority of the biopolymeric structures remain unaltered, preserving their surface topography, size, mechanical properties, and degradation profiles.

Comprehending the surface chemistry of SMCs, fine-tuning their properties, and unravelling potential mechanisms are essential for maximizing their effectiveness and biocompatibility. Therefore, we directed our focus toward two key aspects: i) extracting SMCs with diverse sizes and surface architectures sourced from bee pollen pellets, while customizing the surface hydrophilicity to establish functionality, and ii) assessing the biocompatibility of SMCs through an *in vitro* cytotoxicity test, exploring the specific interactions of SMCs with biological elements such as cancer cells.

2. Materials and methods

2.1. Chemicals and materials

Orthophosphoric acid (85 % aqueous solution), hydrochloric acid (analytical reagent grade), sodium hydroxide (analytical reagent grade), disodium hydrogen phosphate (analytical reagent grade), monopotassium phosphate, ethanol (absolute, ≥99.8 %), methanol (HPLC grade, ≥99.8 %), acetone (analytical reagent grade, ≥99.8 %), and diethyl ether (analytical reagent grade, ≥99.5 %) were purchased from Fisher Scientific (Pittsburgh, PA, USA). Sodium chloride (ACS grade) and potassium chloride (ACS grade) were purchased from Panreac Applichem (Barcelona, Spain). DPPH, formaldehyde, and glutaraldehyde were acquired from Sigma-Aldrich (St. Louis, MO, USA). Epifluorescence mounting medium containing 4′-6-diamidino-2-phenylindole (DAPI) was purchased from Vector Laboratories, Inc. (CA, USA). While Dulbecco's Modified Eagle Medium (DMEM) was purchased from PAN-Biotech (Aidenbach, Germany), Roswell Park

Memorial Institute (RPMI) 1640 medium was purchased from Corning, Inc. (NY, USA). Triton-X100 and phalloidin were purchased from Invitrogen (Thermo Fisher Scientific, MA, USA). Water was treated using a Milli-Q water purification system (TGI Pure System, TX, USA).

2.2. Sample collection and preparation

In our prior investigation, we provided a comprehensive account of the bee pollen collection, processing, purification, and plant species identification processes [19,20]. In summary, the bee pollen samples were gathered from *Apis mellifera iberiensis* hives located in Bragança, Portugal, in 2022. The collected bee pollen pellets, obtained using a pollen trap, underwent an initial cleaning phase to remove wood residues and dead bee parts. Subsequently, under the scrutiny of a light microscope (Nikon Microphot-FXA, Nikon Co., Tokyo, Japan), the bee pollen samples were meticulously examined to identify specific pollen pellets of interest. These identified pellets were then separated by color. After this initial separation, a palynological analysis was conducted to unveil the botanical origins of each bee pollen pellet, separated by color, and ascertain their purity. The samples were stored at –22 °C until the time of further analysis.

2.3. Defatting of bee pollen pellets and purification of SMCs

Initially, 50 g of bee pollen was placed in a round-bottom flask and underwent reflux in 400 mL of acetone at 50 °C with agitation at 220 rpm for 3 h, Fig. 1 [16]. The supernatant was then decanted, and the samples were thoroughly washed with 400 mL of warm water at 50 °C, maintaining agitation at 220 rpm for 1 h; this washing step was repeated twice. Subsequently, the resulting sample was subjected to another round of reflux in 400 mL of acetone at 50 °C with agitation at 220 rpm for 3 h. After removing the acetone, the sample was air-dried for 12 h in a fume hood. Next, the dry sample was stirred in 400 mL of diethyl ether at room temperature with agitation at 300 rpm for 2 h, and this stirring step was repeated twice. The sample was further washed with 400 mL of fresh diethyl ether at room temperature, using a magnetic stirrer for 12 h. After each supernatant removal, pollen particles were collected using an oil-free vacuum pump (Rocker 400, Rocker Scientific Co., Ltd., New Taipei City, Taiwan), passing the solution through a glass filter with a diameter of ϕ5-11 μm. The sample was then dried in a fume hood for an additional 12 h.

Defatted pollen grains were subjected to acidolysis in 400 mL of phosphoric acid (70 °C, 250 rpm) for 8 h as described elsewhere [17]. Post-acidolysis, the SMCs were subjected to a series of 400 mL washing steps at 50 °C, including water, acetone, 2 M hydrochloric acid, 2 M sodium hydroxide, and ethanol. SMCs were collected by vacuum filtration after each washing step. Samples were transferred to a glass Petri dish and dried in an oven (Memmert UNE400, Schwabach, Germany) at 45 °C for 3 days. The dried SMCs were then stored in a dry ambient at room temperature.

2.4. Applied procedures for surface change of SMCs

2.4.1. UV-C irradiation treatment

SMCs were irradiated at room temperature within a UV-ABC cabinet (UV-Consulting Peschl España S.L., Geldo, Spain) using a low-pressure mercury lamp (PUV LD450) at a wavelength of 254 nm [22]. The samples were exposed for 24 h, positioned 10 cm from the light source. The radiation intensity was 3.20 J/cm^2, and the temperature reached a maximum of 28 °C during the treatment. The dose of incident radiation during 1 h of exposure was 3.17 W/cm^2.

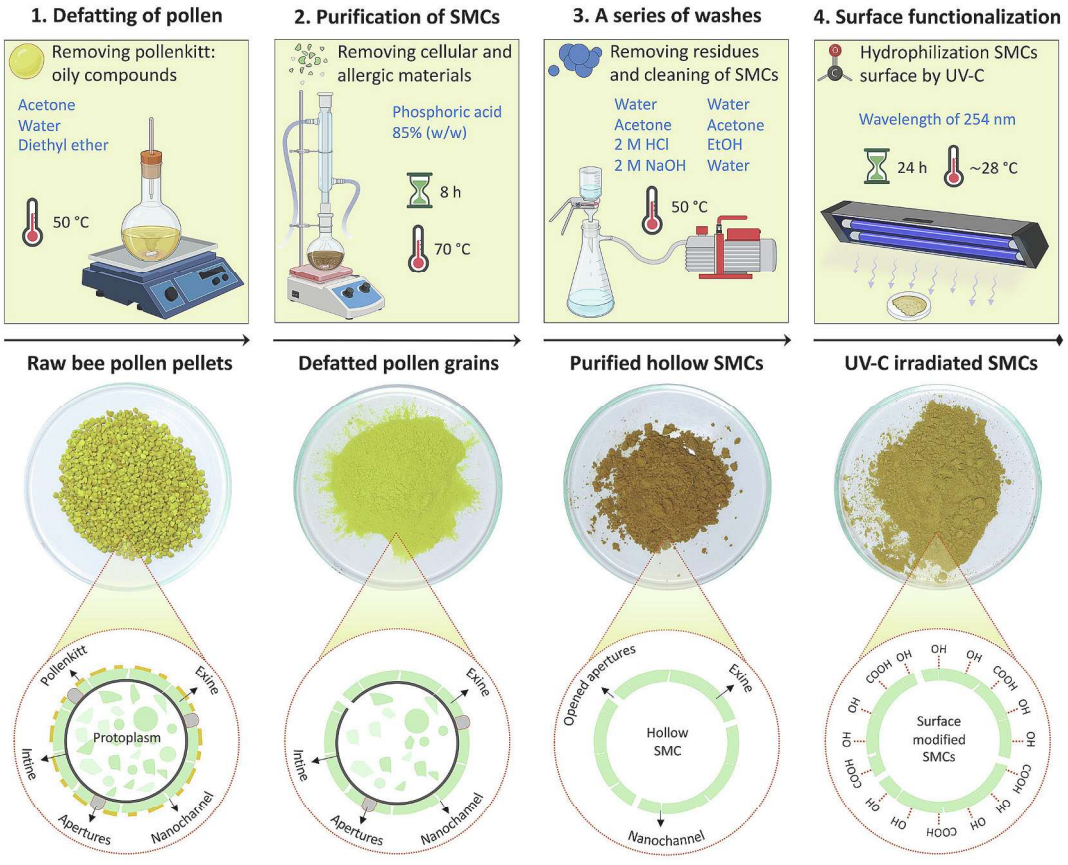

Fig. 1. Schematic diagram illustrating surface modification of natural SMCs by UV-C irradiation following defatting, acidolysis, and washing of bee pollen pellets, resulting in enhanced wetting properties.

2.4.2. Alkaline treatment

The dry SMCs were subjected to an alkaline solution according to a method previously reported elsewhere [25]. Approximately 2 g SMCs were refluxed in 20 mL of 2 M sodium hydroxide (80 °C, 200 rpm) for 4 h. After, the samples were washed with ethanol until a colorless filtrate was obtained and dried in an oven at 45 °C for 3 days.

2.5. Contact angle measurement

Contact angle measurements were performed on untreated SMCs as well as those treated with UV-C irradiation. To facilitate the measurements, a glass slide was prepared with double-sided adhesive tape, and a thin layer of SMCs was evenly spread on the tape's top surface [8]. A drop of water (3 μL, at room temperature) was delicately dropped onto the surface of the samples. Contact angles were then measured through filming and photography using an Attension ThetaOptical Tensiometer (Biolin Scientific, Gothenburg, Sweden) equipped with the OneAttension software.

2.6. AFM analysis

AFM was employed for nanoscale surface visualization and surface roughness calculation of the samples. Samples were fixed to a flat mica surface using a commercially available brand of nail polish (Golden Rose, Istanbul, Turkey) based on nitrocellulose and polyvinyl butyral resin. AFM imaging was carried out at room temperature in tapping mode using an AFM model TT-AFM (AFM Workshop, SC, USA) instrument, equipped with a nominal tip radius of < 10 nm (ACT, AppNano, CA, USA), with a resonance frequency of around 300 kHz. Images were preprocessed using Gwyddion 2.4 software.

2.7. FTIR spectroscopy

FTIR measurements were conducted using the Summit X FTIR Spectrometer (Thermo Scientific Corp., MA, USA), which was equipped with a monolithic diamond crystal attenuated total reflection (ATR) accessory. Reflectance infrared spectra were obtained at a spectral resolution of 4 cm^{-1}, with 64 scans performed per measurement spanning the range from 4000 to 600 cm^{-1}. Background spectra were collected before reading the sample. The data were processed using the OMNIC Paradigm Desktop Software (Thermo Scientific Corp.).

2.8. XPS spectroscopy

XPS was used to characterise the surface chemistry of SMCs and UV-C-treated SMCs. XPS was performed using a K-Alpha system (Thermo Fisher Scientific, MA, US) equipped with a monochromatic Al Kα source (1486.6 eV). The X-ray source was oriented at a 60° angle relative to the sample surface normal, and spectra were acquired in constant analyzer energy mode. Charge compensation was applied using a dual low-energy electron and ion flood gun system, angled at 58° from the sample normal. Survey and high-resolution spectra were collected to determine elemental composition and chemical states.

2.9. Reaction of SMCs with DPPH•

A specific volume of a 60 μM DPPH• methanol solution was added to achieve a concentration of 0.3 mg/mL with 10 mg of untreated and UV-C-treated SMCs, following the literature [29]. To ensure the dispersion of individual SMCs in the DPPH• solution, samples underwent vortexing for 3 min, followed by 2 min of ultrasound application. Subsequently, the samples were placed in a dark environment at room temperature for 30 min. Post-incubation, SMCs were separated from the solution using a 0.22 μm membrane filter. Spectrophotometric data were collected by using a UV/Vis spectrophotometer (Zuzi 4255/50, Auxilab Co., Navarra, Spain) in the 200–900 nm wavelength region and processed through the UV/Vis Analyst software (Auxilab Co., Navarra, Spain).

2.10. Biocompatibility and cancer cell adhesion studies of SMCs

The biocompatibility of untreated and UV-C-treated SMCs was assessed through the sulforhodamine B assay using the kidney of the Vero, a non-tumor cell line. The cell line was obtained from the European Collection of Authenticated Cell Cultures (ECCAC). Cells were cultured in DMEM containing heat-inactivated fetal bovine serum (10 %), glutamine (2 mM), penicillin (100 U/mL), and streptomycin (100 μg/mL) at 37 °C with humidified air and 5 % CO_2. Adherent cell cultures were treated with trypsin for cell detachment and dispersal before the assays. Each cell line, prepared at a density of 1.0×10^4 cells/well in 48-well plates, was incubated for 24 h to ensure attachment. Sample concentrations ranging from 0.125 to 8 mg/mL in water were added and incubated for an additional 48 h. Dose-response curves were generated and used to calculate growth inhibition 50 (GI_{50}) values (μg/mL), representing the concentration inhibiting 50 % of cell growth. Each sample was tested in two independent experiments, with each experiment performed in duplicate.

The investigation into cell binding in untreated and UV-C-treated SMCs involved the use of the human colorectal adenocarcinoma cell line – Caco-2. The cell line was obtained from the ECCAC. To achieve sterilization, SMCs samples underwent incubation in diethyl ether and subsequent drying to a stable weight in a vacuum oven at 25 °C. Cultured cells (200,000 cells per well) in RPMI 1640 medium containing 10 % fetal bovine serum, 2 mM glutamine, 100 U/mL penicillin, and 100 μg/mL streptomycin were directly grown on coverslips within a 6-well tissue culture plate, maintaining a temperature of 37 °C and 5 % CO_2. The incubation period of 24 h was allowed for cells to adhere to coverslips. The culture medium was replaced with 2 mL of fresh culture medium containing approximately 50,000 particles (~1.6 mg of SMCs), initiating another 24 h of incubation for subsequent analysis of cell interactions with the introduced SMCs samples. Following incubation, samples underwent a gentle 3 times washing, each lasting 3 min, with 3 mL of 1 × phosphate-buffered saline (PBS) at 37 °C. Subsequently, cells were stained for actin filaments and nuclei using phalloidin and DAPI, respectively. To initiate this process, 3 mL of 3.7 % formaldehyde was added to fix the cells on the coverslip and incubated for 7 min. The fixed cells were then washed 3 times (each for 3 min) with 1 × PBS. To permeabilize the cells, a solution of 0.1 % Triton-X100 in 1 × PBS was applied and left to incubate for 5 min, followed by another 3 times washing (each for 3 min) with 1 × PBS. Next, the cells were incubated in a phalloidin solution (1:100) for 30 min at room temperature and washed twice (each for 3 min) with 1 × PBS at the end of the incubation period. Finally, a drop of antifade mounting medium containing DAPI was applied to the microscope slide, and the coverslip with the sample was positioned on the slide and examined under the confocal microscope.

2.11. Imaging analyses

Changes in the surface structure of samples were examined using a SEM, FEI Quanta 400 FEG ESEM/EDAX Genesis X4M instrument (FEI Inc., OR, USA) with a 15.00 kV acceleration voltage, employing various magnifications. To capture images, samples were spread on conductive carbon tapes and coated with Au/Pd using a sputter coater (SPI Module Sputter Coater, PA, US) at 15 mA for 100 s. For the cell study, SMCs/cells underwent fixation with glutaraldehyde (4 %, 40 min), followed by three washes with 1 × PBS (5 min each). Subsequently, a sequential ethanol dehydration process (ethanol 25 %, 50 %, 75 %, 95 %, 100 % for 20 min each) was carried out, followed by freezing at −80 °C for 12 h and freeze-drying for 24 h.

CLSM was used for visualizing both the samples (inherently autofluorescent) and the cells. SMCs samples were spread on a glass slide with a drop of epifluorescence mounting medium containing DAPI, and

mounted with a coverslip. LSM 510 META with a Zeiss Axio Imager Z1 (Carl Zeiss, Jena, Germany) and the LSM 510 software (version 4.0 SP2) were used to acquire confocal images. The same settings were applied to all images for results normalization. The lasers used were argon (488 nm) set at 13 %, helium–neon (543 nm) set at approximately 51 %, and diode (405 nm) set at approximately 39 %. The pinhole was set to 96 mm (1.02 airy units) for the argon laser, 102 mm (0.98 airy units) for the helium–neon laser, and 112 mm for the diode laser using a 63 × objective. Images were captured at a scan speed of 6 or 8 with 1 μm thick *z*-sections, deconvolutioned using the three-dimensional (3D) deconvolution tool of the AutoQuant X3 software (Media Cybernetics Inc., MD, US), and processed in TIFF images with ImageJ (1.47v).

2.12. Statistical analysis

Data analysis was performed using GraphPad Prism version 9.5.1 (San Diego, CA, USA). The two-tailed *t*-test was employed for comparisons between two groups, while one-way ANOVA with post hoc Tukey test was utilized for comparisons among three or more groups. Significance levels of the *p*-value are denoted as follows: 0.01 to 0.05 (*), 0.001 to 0.01 (**), and < 0.001 (***). Values are presented as mean ± standard error.

3. Results and discussion

3.1. Extraction of SMCs from bee pollen pellets

Solvent extraction with acetone, water, and diethyl ether effectively removed residues, including the pollenkitt, which forms the oily layer on top of the exine wall. This process produced discrete particles, as shown in Fig. 1. Defatting, acidolysis, and successive washing steps produced hollow and clean SMCs, as shown in the SEM images, Fig. S1. This method sufficiently removed cellular material from all pollen species. Importantly, the extraction process preserved the 3D shape of the pollen grains, maintaining their intact structure and surface morphology. Another observation was that apertures in the pollen wall opened after acid treatment. These areas typically have an inner layer called the intine. The acid entering the pollen's inner cavity creates internal pressure, eventually causing the pollen wall to break in the areas with apertures. The very thin or absent exine layer in these regions is considered the primary factor responsible for this phenomenon [16].

3.2. Hydrophilicity modulation and surface topography

Hydrophobic micro or nanospheres are well suited for stabilizing molecules with limited water affinity; however, biological compatibility generally depends on hydrophilic components, which facilitate cell adhesion and enhance tissue residence time [30]. There are various strategies, including radiation, to convert hydrophobic structures into hydrophilic ones. Among the various radiation-based surface modification strategies, UV-C treatment stands out as a dry, efficient, and cost-effective approach applicable across industrial and biological fields. UV-C induced surface modification has been widely investigated for its ability to alter material properties, with applications ranging from surface disinfection of packaging materials to biomaterial functionalization [11,27,28,31]. In the context of biomaterials, UV-C irradiation can modify surface characteristics, enhancing properties such as wettability, roughness, and chemical reactivity [22]. We hypothesize that UV-C irradiation treatment could significantly alter the surface properties of SMCs, particularly in their outer wall (exine), where UV absorption predominantly occurs. In addition to modifying the surface chemistry of the SMCs using UV-C treatment, we also explored the use of 2 M sodium hydroxide to improve water wettability and to compare the effects of both treatments.

The surface chemistry of SMCs is recognized for its amphiphilic behavior [8], yet most reports describe them as hydrophobic [9,16,25]. In Fig. 2 and Fig. S2 of the Supplementary Information, we presented time-dependent water contact angle measurements (at intervals of 0, 1, 3, and 5 min) for seven distinct types of untreated and UV-C-treated SMCs, and included optical microscope images illustrating time-dependent water droplets for all samples. The findings showed the hydrophobic nature of all untreated samples, except for the Hel type of SMCs, as evidenced in the fifth-minute measurement, Figs. 2a-2d. As seen in the micrographs of the Cas type SMCs in Fig. 2e, the water contact angle exhibited minimal variation over time, and other samples without treatment showed a similar trend. Statistically significant differences ($p < 0.05$) were observed between UV-C-treated and untreated SMCs, except for the Cas and Jasi samples at the initial time point. The UV-C-treated SMCs exhibited superhydrophilic behavior within the first minute, showing almost no measurable contact angle by the third and fifth minutes. As illustrated in Figs. 2e and 2f, micrographs taken after the first minute show clear differences between UV-C-treated and untreated SMCs, with the effects of irradiation visibly distinguishable. Moreover, none of the SMC samples treated with sodium hydroxide exhibited significant wettability toward water, Fig. S3. A previous study has reported that the carboxyl groups of SMCs derived from pine pollen become deprotonated under alkaline conditions, resulting in superhydrophilicity [25]. Although these findings suggested that the sporopollenin biopolymer contributes to hydrophilic behavior, they primarily attributed this property to the presence of the intine layer, which is composed mostly of cellulose and pectin. It is important to clarify that the intine layer is not part of the sporopollenin biopolymer. In our study, time-dependent water contact angle measurements of seven different SMC types after alkali treatment did not show comparable hydrophilic behavior. This suggests that sodium hydroxide treatment did not alter the inherent chemical inertness of our SMCs. Therefore, we limited our focus to UV-C-treated SMCs for further investigation.

Surface roughness is seen as a physical parameter that can have a significant impact on changing the wettability of materials [22]. To evaluate whether the superhydrophilicity observed in UV-C-treated SMCs is influenced by surface roughness, we employed AFM, a highly sensitive technique for characterizing surface topography at the micro and nanometer scale, and compared the results with those of untreated SMCs. To complement this analysis, SEM was used to evaluate the overall morphology and microstructural surface features of the SMCs.

As demonstrated by SEM and AFM imaging, Figs. 3a and 3b. UV-C treatment did not induce significant modifications in the overall surface architecture of SMCs. However, minor morphological changes were observed in some treated SMCs. Nanoscale modifications were more pronounced in the rugulate Cas, perforated Ech, and microechinate Hel type SMCs, as revealed by both SEM and AFM analyses. These observations were further supported by AFM-based surface roughness measurements, which indicated nanoscale differences between untreated and UV-C-treated SMCs, Fig. 3c. Despite these variations, none of the observed changes in surface roughness were statistically significant ($p < 0.05$). Additionally, surface variations in micro- and nano-scale imaging may partly result from the inherent non-uniformity of SMC surface architecture. Tapping mode-based roughness analysis revealed that Cis SMCs exhibited the highest surface roughness, measured at ~ 60 ± 5 nm, which decreased to ~ 54 ± 5 nm after UV-C treatment. Conversely, Cas type SMCs displayed the lowest roughness, with an initial value of ~ 26 ± 5 nm, decreasing to ~ 16 ± 3 nm following 24 h of UV-C treatment. Apart from Ama type SMCs, surface roughness generally increased with increasing SMCs size (ranging from 12.5 ± 0.1 μm to 36.3 ± 0.1 μm), while UV-C treatment resulted in a smoother surface. Furthermore, SEM micrographs confirmed that UV-C irradiation did not alter the overall 3D microstructure of the SMCs, Fig. S4.

The effects observed in this work align with previous findings on UV-induced surface activation of both synthetic and biologically derived polymers. It has been reported that UV-C treatment enhances the water affinity of biopolymers, including collagen/elastin [22], starch [11], polylactic acid [27], chitosan, and silk fibroin [26], in some cases

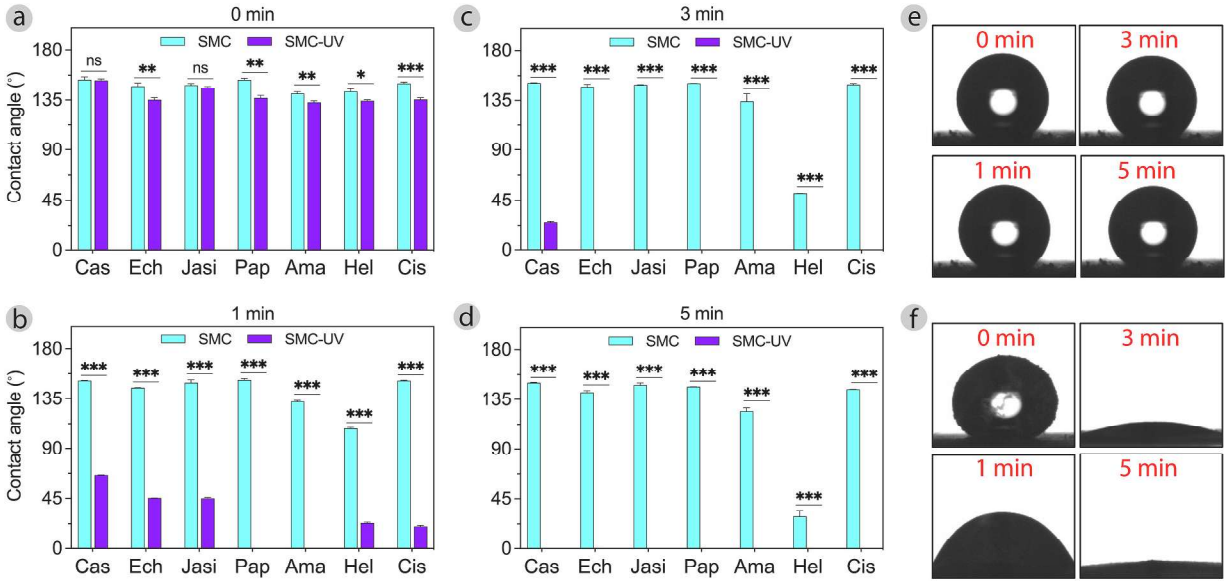

Fig. 2. Contact angle analysis of untreated and UV-C-treated SMCs over time: (a) Initial contact angle at 0 min, (b) at 1 min, (c) at 3 min, and (d) at 5 min; optical images of water droplet formation on (e) untreated Cas type SMCs and (f) UV-C-treated Cas type SMCs. Data is presented as mean ± standard deviation (n = 3). The *t*-test was used for comparisons. Statistical significance is indicated as follows: 0.01 to 0.05 (*), 0.001 to 0.01 (**), and < 0.001 (***). ns: not significant.

accompanied by a reduction in surface roughness and improved interaction with biological materials [22,26]. Water contact angle measurements confirmed that SMCs became superhydrophilic following UV-C irradiation. However, AFM and SEM analyses revealed that nanoscale surface changes were insufficient to explain this behavior, pointing instead to underlying chemical modifications as the primary cause.

3.3. *UV irradiation causes structural changes in SMCs by altering surface chemistry*

Following the evaluation of water contact angles, SEM analysis, 3D nano mapping, and surface roughness measurements, we performed FTIR and XPS analyses to understand the impact of the applied UV-C treatment on the surface chemical structure of SMCs, thereby elucidating the mechanisms underlying their enhanced affinity for water. Sporopollenin, a highly resistant biopolymer, contains phenolic compounds such as *p*-coumaric acid and ferulic acid, which contribute to its structural integrity through cross-links with aliphatic chains [32,33]. These phenolic compounds also enable longer wavelengths of UV-A and UV-B absorption via their aromatic rings, protecting the material from photodegradation [34]. However, UV-C irradiation, characterized by its short wavelength and high energy, has the potential to break chemical bonds and induce molecular modifications [22].

The XPS data reveal some changes in elemental composition and carbon/oxygen bonding states across all seven SMCs types, providing a clear chemical basis for the observed wettability shift. The XPS high-resolution spectra of C and O, Fig. 4, demonstrate an increase in surface oxygen content and a corresponding decrease in carbon content after UV-C treatment. The oxygen-to-carbon (O/C) ratio increased significantly in all SMCs, confirming extensive surface oxidation Fig. 4a and Table S1. The lowest change in the O/C ratio was from 0.17 to 0.21 in the Ech type SMCs (24.5 % increase), and the highest change was from 0.15 to 0.27 in the Pap type SMCs (78.5 % increase). This overall increase in surface oxygen concentration is the primary indicator of oxidative modification induced by prolonged UV-C exposure, which creates a more polar surface [8]. UV-C irradiation, with its high photon energy, is known to break C–C and C–H bonds, leading to the formation of radicals that react with ambient oxygen or moisture to generate hydroxyl, carbonyl, and carboxyl groups [31].

The high-resolution C1s spectra supported this transformation, Fig. 4b and Table S2. A consistent reduction in the relative proportion of non-polar hydrocarbon C–C/C–H bonds (284.8 eV) was observed across all SMCs. For instance, this component decreased from 77 % to 64 % (−14 %) in Hel type SMCs and from 75 % to 67 % (−8%) in Ama type SMCs. At the same time, the relative intensities of oxygenated carbon species increased. Notably, the indicative of hydroxyl or ether (C–O, ~286 eV) formation increased significantly in samples, such as Pap type SMCs (13 % to 20 %, +7%), Hel type SMCs (11 % to 20 %, +9%), and Cas type SMCs (11 % to 15 %, +4%). In addition, the C═O (carbonyl, 286.9 –287.4 eV) and O–C═O (carboxyl/ester, 288.2–288.6 eV) groups showed meaningful increases, particularly in Ama, Hel and Cis type SMCs. The formation of these oxygen-containing groups enhances the hydrophilic character of the surface, facilitating water spreading and absorption [26]. Similar findings have been previously reported with a decrease in atomic carbon concentration and a corresponding increase in oxygen concentration following UV-ozone treatment of *Camellia sinensis* pollen [8].

The O1s spectra further confirm and provide further insight into these modifications, Fig. 4c and Table S3. Carbonyl oxygen (C═O, 531.2–531.6 eV) proportions generally remained high or increased slightly, such as Ech type SMCs (55 % to 62 %), Pap type SMCs (55 % to 62 %), Ama type SMCs (49 % to 61 %), Hel type SMCs (52 % to 65 %), and Cis type SMCs (59 % to 64 %), consistent with C1s data showing stable or increased carbonyl presence in several SMCs. Simultaneously, the proportion of carboxyl/oxygen in esters (O–C═O, ~530.0–531.3 eV) species increased notably in Cas type SMCs (6 % to 14 %) and Pap type SMCs (6 % to 13 %), indicating the formation of carboxylic acid or ester groups. Although hydroxyl/ether oxygen (C–OH, 532.5–532.9 eV) bonds were decreased significantly in some samples (e.g., Cas, Ech, Pap, and Hel type SMCs), this could likely be due to further oxidation of hydroxyl groups into more oxidized species, rather than a reduction in surface polarity. The general trend across C1s (increase in C–O) suggests new hydroxyl formation.

Sample-by-sample analysis shows that the extent of oxidation and polar group formation varied depending on the plant origin of the sporopollenin. The most pronounced chemical changes were observed in Ama, Pap, and Hel type SMCs, which also exhibited the highest increases in oxygen content and polar functionalities. For example, Ama type SMCs had a reduction in C–C/C–H from 75 % to 67 %, with a concurrent rise in O–C═O from 5 % to 10 % and in C═O from 4 % to 6 %. Such

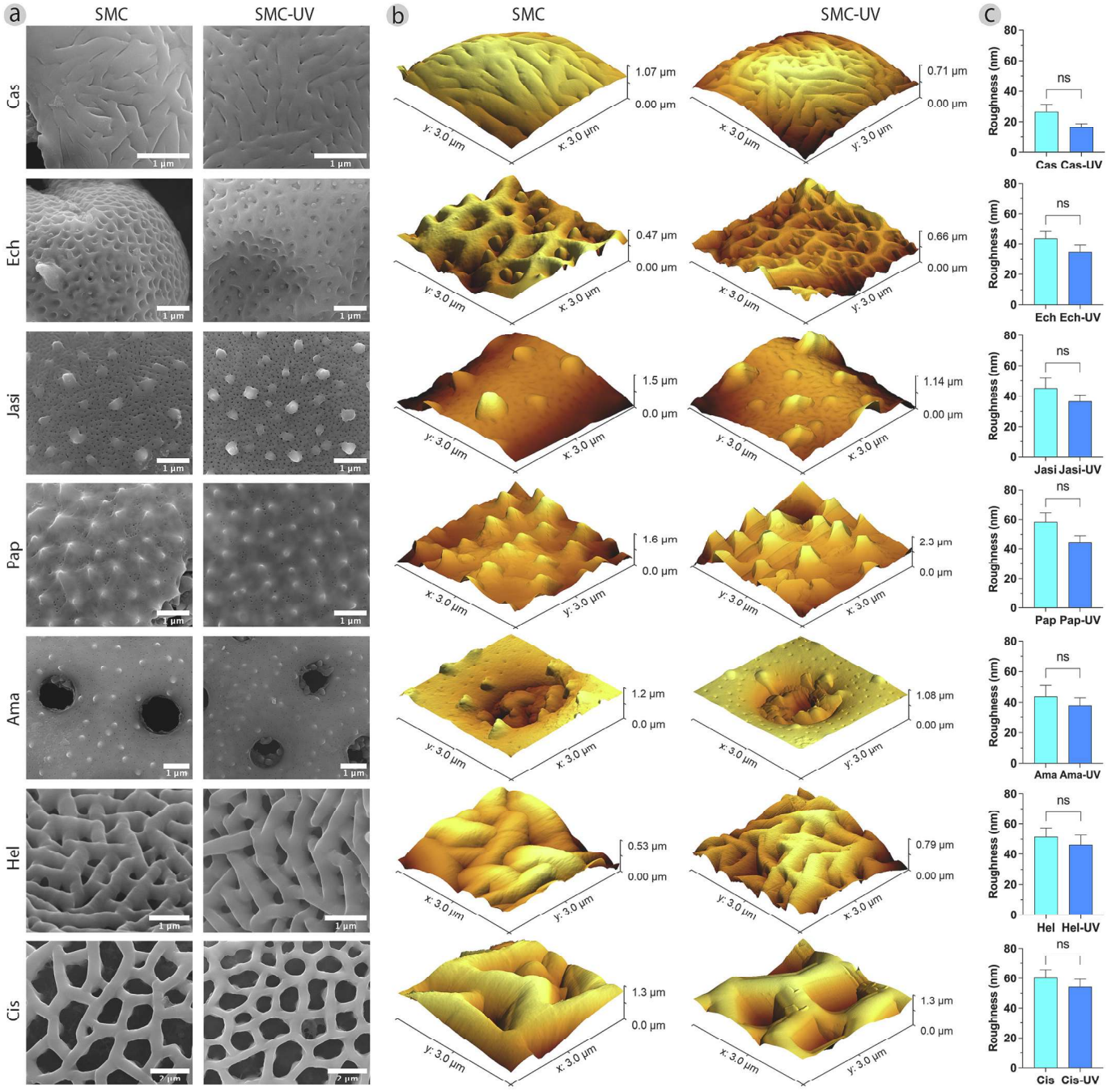

Fig. 3. SEM and AFM images, and roughness of untreated and UV-C-treated SMCs: (a) SEM images of the surface architecture of untreated and UV-C-treated SMCs, (b) AFM 3D surface reconstruction from height trace data of untreated and UV-C-treated SMCs, and (c) surface roughness calculations of untreated and UV-C-treated SMCs. Three pollen grains were measured for each type of SMCs, and two to four measurements were taken from each one. The data is presented as mean ± SD, and the *t*-test was performed for comparison. ns: not significant.

modifications support the enhanced surface wettability and superhydrophilicity [8,25,27]. In summary, UV-C irradiation effectively altered the surface chemistry of all SMCs by introducing a greater density of polar oxygen-containing groups, such as hydroxyl, carbonyl, and carboxyl functionalities, while reducing nonpolar hydrocarbon content. These surface transformations increased the affinity for water, accounting for the observed transition from hydrophobicity to superhydrophilicity [22,26,35].

Moreover, the differences in surface chemistry observed between untreated and UV-C-treated SMCs can be attributed to the inherent chemical and structural heterogeneity of sporopollenin biopolymer from different plant species [33]. Sporopollenin is not a uniform biopolymer but a complex, cross-linked network derived from varying proportions of precursors (carotenoids, phenylpropanoids like *p*-coumaric acid, fatty acids) across plant species [32]. Differences in monomer ratios (aliphatic vs. phenolic) and cross-linking types (ether, ester, and acetal) can dictate the initial surface composition as probed by XPS [33]. For instance, Cas and Hel exhibit higher aliphatic (C–C/C–H) content, which may be due to a sporopollenin structure richer in fatty acid derivatives, while Cis and Jas may be composed of a biopolymeric backbone richer in phenolic precursors due to the higher O/C ratio, Table S1, S2 and S3. The variability within the C–O bonds also allows us to conclude that ether bonds are the most characteristic for all the pollen sporopollenin structures; however, Jas and Pap pollens stand out as biopolymers rich

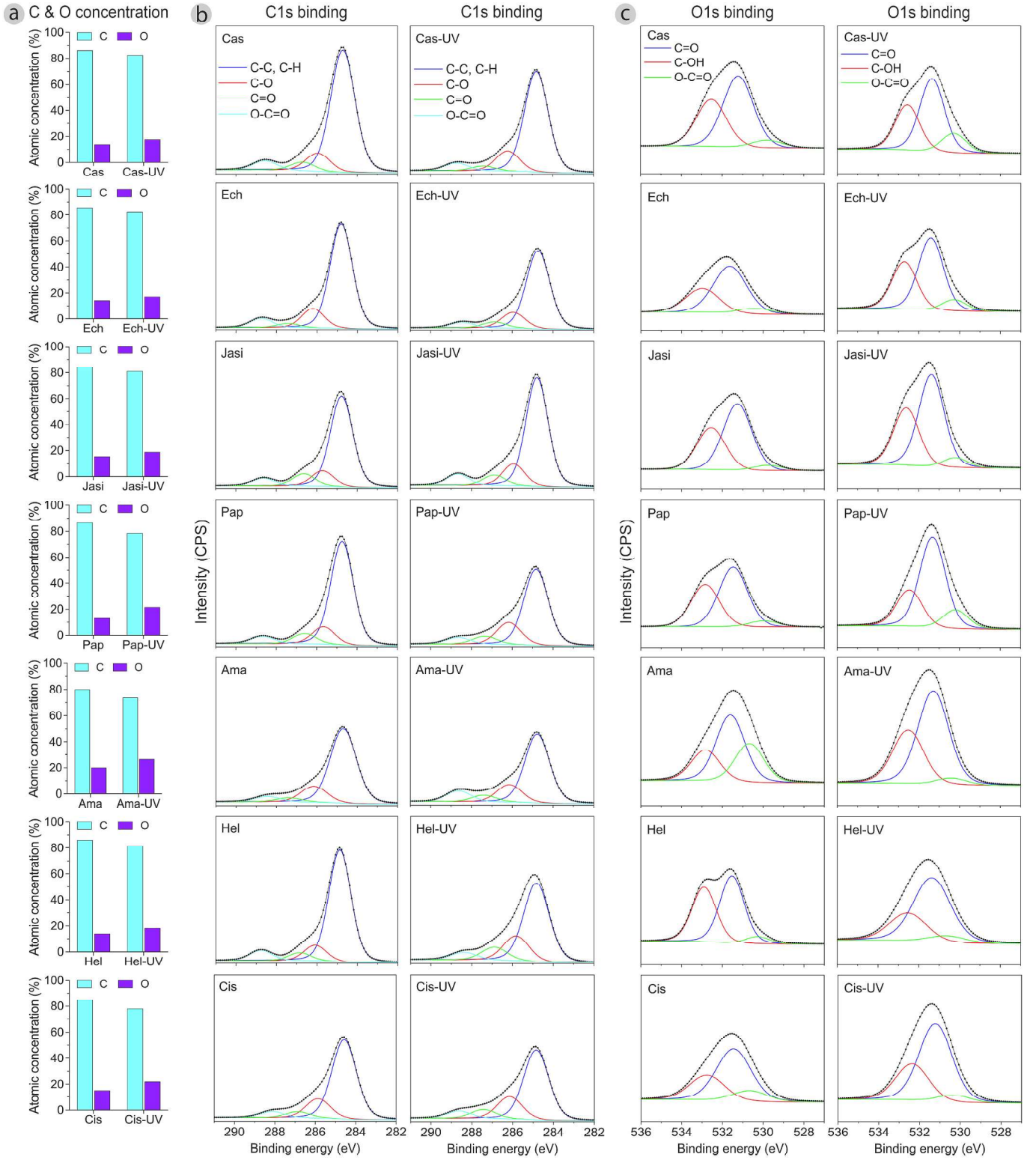

Fig. 4. XPS based surface chemical analysis of untreated and UV-C-treated SMCs: (a) quantification of atomic carbon and oxygen content of untreated and UV-C-treated SMCs, (b) C1s peak-fitting for carbon bonding states of untreated and UV-C-treated SMCs, and (c) O1s peak-fitting for oxygen bonding states of untreated and UV-C-treated SMCs. Dotted black lines represent fitted data.

in acetal bonds, while Ama, Ech, and Hel exhibit higher frequency in ester bonds. Variations in exine structure (thickness, density, nanoporosity) [8] and potential internal chemical gradients influence the effective surface chemistry sensed by XPS (~10 nm depth). Surface roughness and nanoscale features can subtly alter spectral intensities. Sporopollenin can also retain biomolecule residues (proteins, lipids, metabolites) [19] or inorganic impurities (e.g., silica) from the pollen grain or isolation process [8]. Traces of purification chemicals may also persist differently depending on the SMC's surface chemistry. Additionally, SMCs may have a species-specific response to UV-C irradiation

[32]. Sporopollenin richer in oxidizable phenolic groups may follow different radical reaction pathways and form different oxidized products (e.g., alcohols vs. carboxylic acids) compared to more aliphatic types, explaining variations in functional group evolution [8]. Consequently, the baseline surface chemistry and its specific evolution under UV-C treatment are inherently species-dependent, explaining the variations in XPS results despite the universal presence of sporopollenin and its core oxidative response.

ATR-FTIR was employed to investigate general and surface chemical changes in the SMCs induced by UV-C irradiation. Depending on the wavelength and angle of incidence, infrared radiation penetrates the material from approximately 0.5 μm to over 5 μm and can therefore reach from the outer shell of the SMCs to its inner cavity [8]. As a result, detecting structural changes limited to the topmost surface layer of the SMCs may be challenging. Nevertheless, FTIR was used to provide an overall chemical analysis of the SMCs and served as a complementary technique to the surface sensitive XPS analysis.

The spectra of both untreated and UV-C-treated SMCs, Fig. 5, revealed consistent and distinct shifts, confirming the formation of new functional groups and providing supporting evidence for the XPS findings. A broad band around ~ 3370 cm^{-1} attributed to O–H stretching vibrations [32] remained constant or slightly decreased in intensity across all UV-C-treated samples. This confirmed a reduction in hydroxyl (OH) groups, consistent with the general decreasing trend in C–OH signals in the XPS O1s spectra. Similarly, decreased intensities of the aliphatic C–H stretching bands [19] at 2924 cm^{-1} (asymmetric CH_2/CH_3) and 2854 cm^{-1} (symmetric CH_2) indicated a loss of hydrophobic hydrocarbon content, reinforcing XPS observations of reduced C–C/C–H bonds. A prominent increase in the intensity of the ~ 1704 cm^{-1} band, particularly in Jasi, Pap, Ama, Hel, and Cis type SMCs, corresponds to enhanced C═O stretching of carboxylic acids or esters, confirming the formation of hydrophilic acidic groups. This aligns with XPS results showing notable increases in C═O and O–C═O signals in both the C1s and O1s spectra, supporting a photooxidation mechanism responsible for increased surface polarity [26]. Interestingly, the 1704 cm^{-1} and ~ 1675 cm^{-1} peaks, both associated with C═O stretching vibrations, showed varying behavior across the samples. In some SMCs, the original 1675 cm^{-1} peak was substantially reduced or disappeared following UV-C treatment, while a new peak appeared at 1704 cm^{-1}, reflecting the same functional group vibration. These two peaks are assigned to esters or carboxylic acids. A similar spectral shift has been reported in *Camellia sinensis* pollen, indicating structural rearrangements among carbonyl containing groups [8]. The bands at ~ 1580 cm^{-1} and ~ 1515 cm^{-1}, attributed to C═C stretching in conjugated aromatic or phenolic rings [36], remained relatively stable or slightly decreased after UV-C exposure. This suggests that the aromatic backbone of the sporopollenin biopolymer remained largely intact despite oxidative surface modification. Given sporopollenin biopolymer exceptional chemical stability, particularly in its phenolic regions, these minimal changes suggest that the core structure was preserved. The slight decrease at 1580 cm^{-1} may result from minor structural rearrangements. Additionally, variable intensity at ~ 1432 cm^{-1} is attributed to O–H or CH_2 bending, while the ~ 834 cm^{-1} band corresponds to aromatic C–H bending in the sporopollenin backbone [16,25,32].

The general emergence of hydrophilic carbonyl and carboxylate functionalities, coupled with a reduction in aliphatic components, provides a chemical basis for the observed transition to superhydrophilicity. Importantly, these trends were consistent across all seven botanically distinct SMCs, despite differences in oxidation levels. This highlights the robustness of UV-C irradiation as an eco-friendly and effective functionalization strategy for SMCs derived from diverse botanical sources, besides aligning with principles of sustainable biomaterial processing.

3.4. Radical interaction with SMCs

The DPPH$^{\bullet}$ assay is used to evaluate radical scavenging capacity and thus the active functionality of synthetic and natural biopolymers [37,38]. With a distinct absorbance peak at 517 nm, the DPPH$^{\bullet}$ radical may serve as a practical and accessible probe for studying hydrogen or electron-donating functional groups, such as hydroxyl and carboxylic acids [39]. This assay is valuable not only for evaluating antioxidant capacity but also for indirectly detecting newly formed or exposed functional groups after surface modification, or for assessing the presence and antioxidant behavior of compounds incorporated into a host material [37]. A decrease in DPPH$^{\bullet}$ absorbance indicates the presence and reactivity of such groups and their ability to participate in radical interactions.

The DPPH$^{\bullet}$ assay was used in this study to examine the presence and accessibility of functional groups formed on SMC surfaces after UV-C irradiation, Figs. 6a and 6b. While untreated SMCs induced only moderate reductions in DPPH$^{\bullet}$ absorbance, their UV-C-treated counterparts exhibited significantly enhanced radical scavenging activity, evidenced by greater decreases in absorbance at 517 nm. The most pronounced activity was observed in Ama, Pap, Hel, and Cis type SMCs, whereas Cas and Jasi type SMCs showed more modest effects. These results reflect the underlying chemical transformations triggered by UV-C irradiation, as confirmed by XPS analysis. UV-C treatment increased surface oxygenation in all SMCs, although the extent and nature of these changes varied by sample. For example, Ama type SMCs showed substantial increases in surface C═O (from 49 % to 61 %), O–C═O (from 5 % to 10 %), and C–OH (from 23 % to 35 %), reflecting a reduction of 40.1 % in the DPPH$^{\bullet}$ absorbance. These oxygen containing groups, especially hydroxyl and carboxyl moieties, are known to be highly reactive toward DPPH$^{\bullet}$ via hydrogen atom transfer. Similarly, Pap type SMCs exhibited notable increases in C–O (from 13 % to 20 %) and O–C═O (from 6 % to 13 %), supporting their enhanced radical scavenging performance (23.2 % reduction in DPPH$^{\bullet}$ absorbance). This DPPH$^{\bullet}$ scavenging mechanism of SMCs may proceed via possibly two complementary pathways [39,40]: i) Hydrogen atom transfer involves the donation of a hydrogen atom (H$^{\bullet}$) from surface OH or COOH groups to neutralize the DPPH$^{\bullet}$, and ii) single electron transfer involves the transfer of an electron from a donor group such as a conjugated aromatic structure to DPPH$^{\bullet}$, resulting in DPPH^{-}, Fig. 6c.

UV-C irradiation appears to induce surface photooxidation, generating hydrophilic and redox-active groups such as alcohols and carboxylic acids. These functionalities, confirmed by both FTIR and XPS, account for the observed increases in DPPH$^{\bullet}$ reduction. Specifically, samples with higher oxygen incorporation and reduced hydrocarbon content (as reflected by decreased C–C/C–H signals in the C1s spectrum) showed stronger antioxidant performance. Pap, Ama, Hel, and Cis type SMCs exhibited the largest reductions in C–C/C–H content, consistent with successful oxidative surface functionalization. In contrast, Cas and Jasi type SMCs displayed relatively weak DPPH$^{\bullet}$ reactivity after UV-C exposure. For example, Cas type SMCs showed only minor increases in oxygenated groups and even slight reductions in C–OH (from 37 % to 33 %) and C═O (from 57 % to 53 % in the O1s), indicating limited surface oxidation (a 15.3 % reduction in DPPH$^{\bullet}$ absorbance). These samples likely possess more aliphatic or oxidation-resistant compositions, making them less susceptible to UV-C-induced modification.

3.5. Biocompatibility and enhanced cell adhesion of SMCs

Before assessing the interaction of SMCs with Caco-2 type cancer cells, the biocompatibility of both untreated and UV-C-treated samples was evaluated using Vero cells, a non-cancerous cell line commonly used to assess the effects of materials or natural products on cell viability [41,42]. This step was important, as chemical changes induced by UV-C irradiation could potentially exert cytotoxic effects on normal cells. For this purpose, Vero cells were seeded and incubated with various concentrations of both untreated and UV-C-treated SMCs for 48 h. The results showed that GI_{50} > 700 μg/mL for all SMCs types, indicating good biocompatibility. This finding is essential for their safe application in

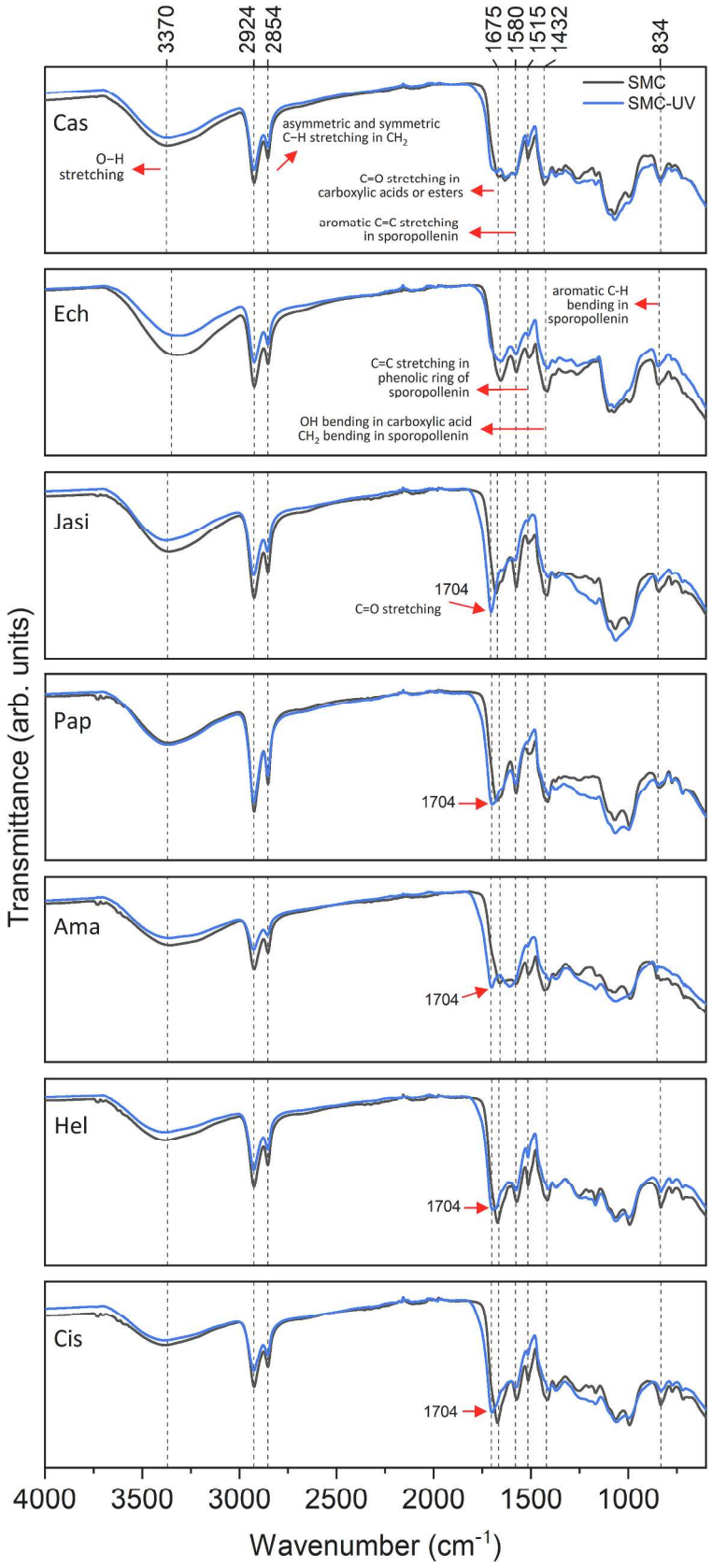

Fig. 5. FTIR spectra illustrating chemical structure changes in SMCs before and after UV-C treatment, including a comparison of major functional group peaks.

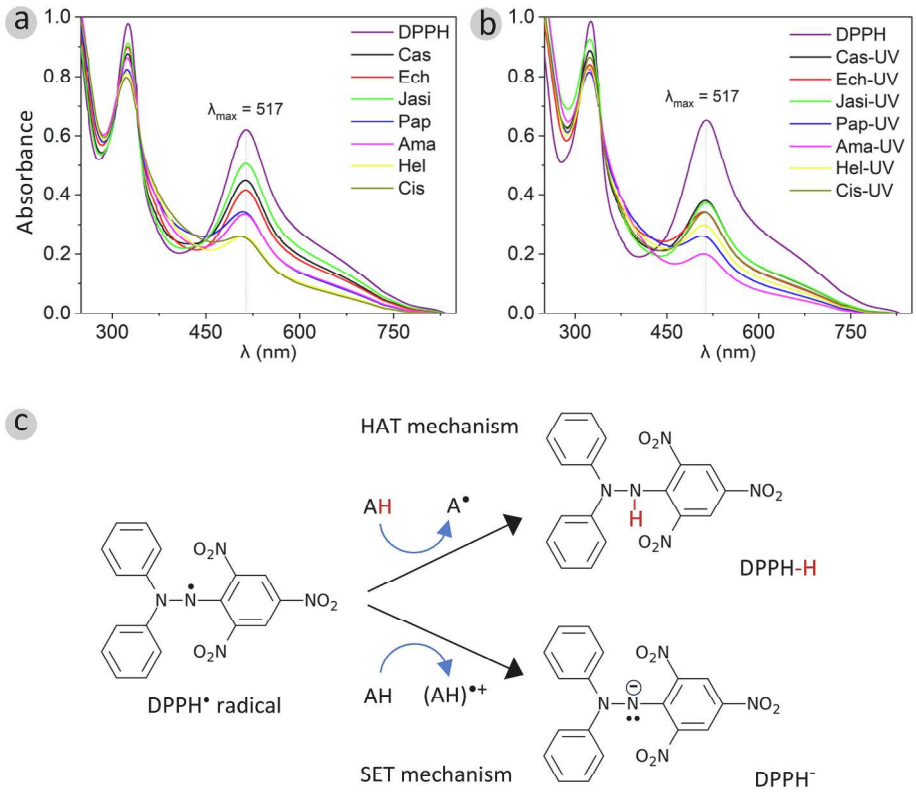

Fig. 6. Reaction of untreated and UV-C-treated SMCs with DPPH•: (a) UV absorption spectra of untreated SMCs after reaction with DPPH•, (b) UV absorption spectra of UV-C-treated SMCs after reaction with DPPH•, and (c) schematic illustration of potential reaction mechanisms SMCs with DPPH•: hydrogen atom transfer (HAT) and single electron transfer (SET).

drug delivery, wound healing, or other therapeutic uses.

To investigate the adhesion properties of the samples to the Caco-2 cells, the cells were first seeded and incubated for 24 h to establish a stable monolayer. The SMCs were then added and incubated for an additional 24 h to assess the cells' adherence to either the untreated or UV-C-treated SMCs. After incubation, the samples were washed to remove poorly attached SMCs, retaining only those firmly attached. SEM images confirmed that loosely bound SMCs were removed, while well-attached ones remained, Fig. 7a. For example, in the SEM image of the untreated Cas type SMCs, the detachment of loosely attached particles is evident from the surface imprint it left on the cell layer, as indicated by the dashed line. Quantification of proportional binding microcapsules by CLSM revealed that UV-C-treated SMCs exhibited from 3 % (Jasi) to 52 % (Cas) higher binding to Caco-2 cells compared to untreated SMCs, Figs. 7b and 7c. This difference was statistically significant ($p < 0.05$) for all SMCs types except for Jasi type SMCs. In the CLSM images, cells are shown in red due to immunostaining with phalloidin and DAPI, while SMCs show an overlay of color at different wavelengths from blue to red due to autofluorescence, Fig. S5 [8]. The images showed filamentous structures originating from the cells that extended to and bound the SMCs. No SMCs were observed in areas lacking cells, confirming that the microcapsules adhered specifically to the cell surfaces. Furthermore, CLSM images showed that untreated SMCs adhered less efficiently to the cells, and regions devoid of SMCs binding were more frequent. Additionally, the internal structure of the SMCs was visualized; the analysis of CLSM *z*-stack slices shows cells and also SMCs in blue, green, and red channels, confirming that the generated SMCs possess a large empty internal cavity, Fig. 8a.

These results underscore that fine-tuning the surface chemistry of SMCs via UV-C irradiation may play a critical role in enhancing cell adhesion and may offer a significant advantage by increasing retention time in intrabody drug delivery systems, Fig. 8b. Previous studies on the UV light functionalization of biomaterials such as natural pollen [8], starch [11], and collagen/elastin [22] have demonstrated that increased cell adhesion can be attributed to the formation of polar groups on the material surface. As noted earlier, the enrichment of SMC surfaces with O–H, C═O, and O–C═O groups following UV-C treatment enhances their hydrophilicity, which supports increased binding to cancer cells. In line with this, previous work has shown that the binding of SMCs coated with polypeptide multilayer films composed of poly-L-lysine hydrobromide and poly-L-glutamic acid sodium salt to human bone marrow-derived stem cells was improved by imparting hydrophilic surface properties [9]. Another factor contributing to SMCs binding to Caco-2 cells may be surface morphology and roughness [43]. Although UV-C treatment did not significantly reduce surface roughness, it did result in smoother surfaces overall. A study by Ranella et al. [44] on fibroblast adhesion to rough 3D silicon surfaces with varying roughness and wettability demonstrated that cell adhesion was greater on smoother silicon surfaces. This suggests that fibroblast adhesion is not solely dependent on surface chemistry and that surface roughness can also play a role.

4. Conclusion

This study demonstrates that UV-C irradiation is an efficient, reagent-free method to overcome the intrinsic bioinertness of natural SMCs. Controlled photochemical oxidation significantly increased surface oxygenation through the introduction of polar oxygen-containing functional groups, as confirmed by FTIR and XPS analyses. These modifications converted the initially hydrophobic SMCs into superhydrophilic structures, with the water contact angle reaching 0° within 3 min. Despite these surface alterations, UV-C treatment preserved the morphological integrity of the SMCs, as evidenced by AFM and SEM micrographs, confirming that changes are limited to the outer surface. Functionally, the UV-C-treated SMCs showed a 52 % increase in adhesion to colorectal cancer cells, compared to untreated SMCs, improving

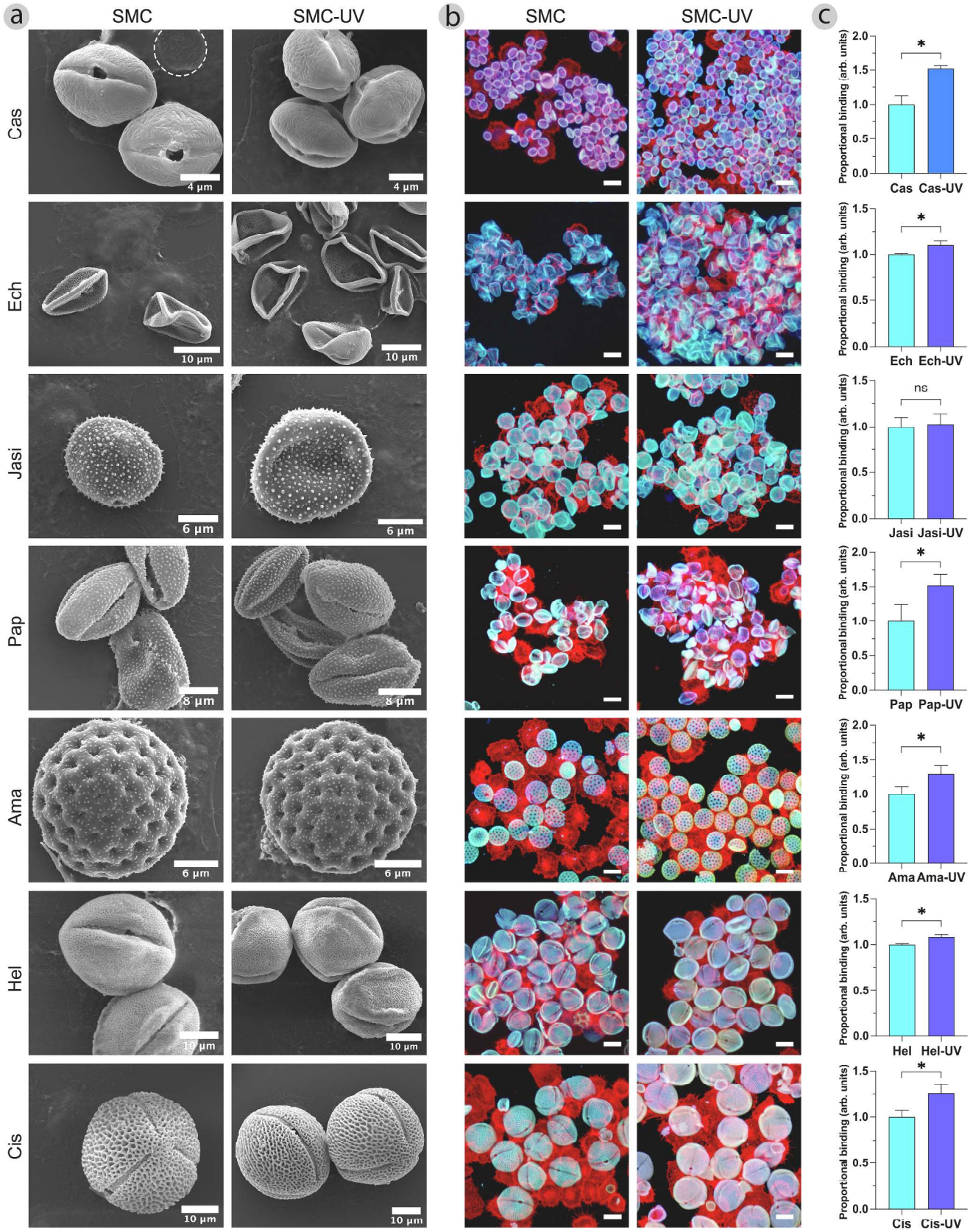

Fig. 7. Evaluation of SMCs binding to Caco-2 colorectal cancer cells: (a) SEM images of interactions between untreated and UV-C-treated SMCs and Caco-2 cells, (b) CLSM overlay images of interactions between untreated/UV-C-treated SMCs and Caco-2 cells, and (c) relative binding of SMCs to Caco-2 cells. Three to five measurements were taken for each SMCs type. The data is presented as mean ± SD, and the *t*-test was performed for comparison. Statistical significance is indicated as follows: 0.01 to 0.05 (*). ns: not significant. CLSM scale bar = 20 µm.

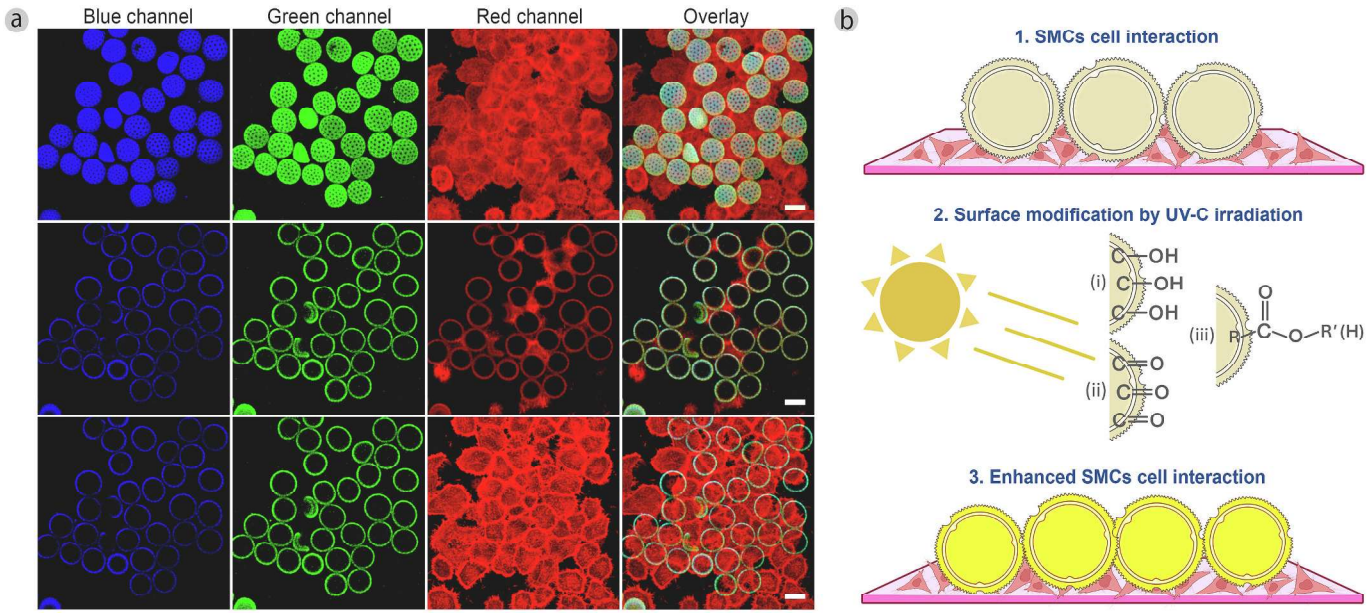

Fig. 8. CLSM based visualization of the interaction between UV-C-treated SMCs and Caco-2 colorectal cancer cells, highlighting the effect of surface chemistry modification: (a) CLSM images of UV-C-treated Ama type SMCs interacting with Caco-2 cells, shown across blue, green, and red fluorescence channels, and also z-stack slices demonstrate the spatial distribution and depth of binding, revealing the hollow internal structure of the SMCs and their localization on or near the cell surface, and (b) schematic representation illustrating the enhanced particle–cell adhesion observed in UV-C-treated SMCs, attributed to increased surface oxygen content and improved hydrophilicity following UV-C exposure. CLSM scale bar = 20 μm.

surface hydrophilicity, while maintaining excellent biocompatibility with healthy cells (GI_{50} > 700 μg/mL). These findings confirm that the hydrophilicity enhancement results primarily from chemical, rather than physical, changes on the surface. Moreover, the clean photochemical nature of UV-C irradiation aligns with the principles of sustainable biomaterial processing, offering an environmentally friendly route for surface functionalization without the use of solvents or reagents.

Collectively, this work establishes UV-C irradiation as a scalable, controllable, and sustainable strategy to tailor the surface chemistry of natural SMCs for biointerface applications. The enhanced hydrophilicity and cell adhesion properties make UV-C-treated SMCs particularly suitable for use in drug delivery, tissue engineering, and regenerative medicine. Future studies should optimize irradiation parameters, explore long-term stability and *in vivo* performance, and investigate the functional loading capacity of modified SMCs to further expand their translational potential in biointerface engineering.

CRediT authorship contribution statement

Volkan Aylanc: Writing – review & editing, Writing – original draft, Visualization, Methodology, Investigation, Formal analysis, Conceptualization. **Andreia F. Peixoto:** Writing – review & editing, Validation, Methodology, Investigation. **Ricardo C. Calhelha:** Writing – review & editing, Methodology. **Olívia S.G.P. Soares:** Methodology, Investigation. **Nuno Vale:** Writing – review & editing, Validation, Supervision, Methodology. **Cristina Freire:** Writing – review & editing, Supervision, Methodology. **Miguel Vilas-Boas:** Writing – review & editing, Supervision, Resources, Project administration, Methodology, Conceptualization.

Declaration of competing interest

The authors declare that they have no known competing financial interests or personal relationships that could have appeared to influence the work reported in this paper.

Acknowledgments

The authors are grateful to the Foundation for Science and Technology (FCT, Portugal) for financial support by national funds FCT/MCTES to CIMO (UIDB/00690/2020 and UIDP/00690/2020), SusTEC (LA/P/0007/2021), and also projects: UIDB/04033/2020, and UIDP/50006/2020. Thanks to national PT national funds UID/50006 - Laboratório Associado para a Química Verde - Tecnologias e Processos Limpos (FCT/MECI, Fundação para a Ciência e Tecnologia and Ministério da Educação, Ciência e Inovação) for UIDB/50006/2020 project. Thanks to national funding, FCT for CEEC contract (2020.01614.CEECIND/CP1596/CT0007) with Andreia F. Peixoto and the Ph.D. research grant for Volkan Aylanc (2021.07764.BD). Thanks to the NextGenerationEU recovery funds through the scope of Project BeeLand 10/C05-i03/2021.PPRR-C05-i03-I-00008.

Appendix A. Supplementary data

Supplementary data to this article can be found online at https://doi.org/10.1016/j.apsusc.2025.165243.

Data availability

Data will be made available on request.

References

[1] M.G. Bah, H.M. Bilal, J. Wang, Fabrication and application of complex microcapsules: a review, Soft Matter 16 (2020) 570–590, https://doi.org/10.1039/C9SM01634A.
[2] T. Maric, M.Z.M. Nasir, N.F. Rosli, M. Budanović, R.D. Webster, N.J. Cho, M. Pumera, Microrobots derived from variety plant pollen grains for efficient environmental clean up and as an anti-cancer drug carrier, Adv. Funct. Mater. 30 (2020) 2000112, https://doi.org/10.1002/adfm.202000112.
[3] V. Aylanc, A.F. Peixoto, N. Vale, C. Freire, M. Vilas-Boas, Sporopollenin-based biomicrocapsules as green carriers for controlled delivery of pharmaceutical drugs, Appl. Mater. Today 33 (2023) 101860, https://doi.org/10.1016/j.apmt.2023.101860.

[4] L.C. Corrêa-Filho, M. Moldão-Martins, V.D. Alves, Advances in the Application of Microcapsules as Carriers of Functional Compounds for Food Products, Appl. Sci. 9 (2019) 571, https://doi.org/10.3390/app9030571.

[5] A. Bilgic, A. Cimen, M. Bayrak, A.N. Kursunlu, Novel optical microcapsule sensor for effective recognition of Hg(II) and Ag(I) ions in the aquatic environments, Opt. Laser Technol. 181 (2025) 111839, https://doi.org/10.1016/j.optlastec.2024.111839.

[6] V. Kozlovskaya, A. Alford, M. Dolmat, M. Ducharme, R. Caviedes, L. Radford, S. E. Lapi, E. Kharlampieva, Multilayer microcapsules with shell-chelated 89Zr for PET imaging and controlled delivery, ACS Appl. Mater. Interfaces 12 (2020) 56792–56804, https://doi.org/10.1021/acsami.0c17456.

[7] J.Y. Choi, B.Y. Yun, Y.U. Kim, Y. Kang, S.C. Lee, S. Kim, Evaluation of thermal/acoustic performance to confirm the possibility of coffee waste in building materials in using bio-based microencapsulated PCM, Environ. Pollut. 294 (2022) 118616, https://doi.org/10.1016/j.envpol.2021.118616.

[8] E.L. Tan, M.G. Potroz, G. Ferracci, J.A. Jackman, H. Jung, L. Wang, N.J. Cho, Light-induced surface modification of natural plant microparticles: toward colloidal science and cellular adhesion applications, Adv. Funct. Mater. 28 (2018) 1707568, https://doi.org/10.1002/adfm.201707568.

[9] S. Zhou, D. Wu, Z. Xu, Q. Jiang, Sporopollenin exine capsules with polypeptide multilayer films promoting cell adhesion, Chem. Eng. J. 475 (2023) 145607, https://doi.org/10.1016/j.cej.2023.145607.

[10] A.R. Patel, C. Remijn, A.I.M. Cabero, P.C.M. Heussen, J.W.M.S. Ten Hoorn, K. P. Velikov, Novel all-natural microcapsules from gelatin and shellac for biorelated applications, Adv. Funct. Mater. 23 (2013) 4710–4718, https://doi.org/10.1002/adfm.201300320.

[11] I. Pashkuleva, A.P. Marques, F. Vaz, R.L. Reis, Surface modification of starch based biomaterials by oxygen plasma or UV-irradiation, J. Mater. Sci. - Mater. Med. 21 (2010) 21–32, https://doi.org/10.1007/s10856-009-3831-0.

[12] R.J. Hickey, A.E. Pelling, Cellulose biomaterials for tissue engineering, Front. Bioeng. Biotechnol. 7 (2019) 428253, https://doi.org/10.3389/fbioe.2019.00045.

[13] M. Gomez-Florit, A. Pardo, R.M.A. Domingues, A.L. Graça, P.S. Babo, R.L. Reis, M. E. Gomes, Natural-based hydrogels for tissue engineering applications, Molecules 25 (2020) 5858, https://doi.org/10.3390/molecules25245858.

[14] E. Kabir, R. Kaur, J. Lee, K.H. Kim, E.E. Kwon, Prospects of biopolymer technology as an alternative option for non-degradable plastics and sustainable management of plastic wastes, J. Clean. Prod. 258 (2020) 120536, https://doi.org/10.1016/j.jclepro.2020.120536.

[15] R.C. Mundargi, M.G. Potroz, S. Park, J.H. Park, H. Shirahama, J.H. Lee, J. Seo, N. J. Cho, Lycopodium spores: a naturally manufactured, superrobust biomaterial for drug delivery, Adv. Funct. Mater. 26 (2016) 487–497, https://doi.org/10.1002/adfm.201502322.

[16] M.J. Uddin, N. Abidi, J. Warzywoda, H.S. Gill, Investigation of the fate of proteins and hydrophilicity/hydrophobicity of lycopodium clavatum spores after organic solvent-base-acid treatment, ACS Appl. Mater. Interfaces 11 (2019) 20628–20641, https://doi.org/10.1021/acsami.9b03040.

[17] T. Fan, J.H. Park, Q.A. Pham, E.L. Tan, R.C. Mundargi, M.G. Potroz, H. Jung, N. J. Cho, Extraction of cage-like sporopollenin exine capsules from dandelion pollen grains, Sci. Rep. 8 (2018) 1–11, https://doi.org/10.1038/s41598-018-24336-9.

[18] J.H. Cane, V.J. Tepedino, Gauging the effect of honey bee pollen collection on native bee communities, Conserv. Lett. 10 (2017) 205–210, https://doi.org/10.1111/conl.12263.

[19] S. Ertosun, V. Aylanc, A.F. Peixoto, A. Santamaria-Echart, P. Russo-Almeida, C. Freire, M. Vilas-Boas, Structural characterization of microcapsules from common bee pollen for the development of delivery systems, J. Polym. Environ. 33 (2024) 1171–1184, https://doi.org/10.1007/s10924-024-03478-0.

[20] V. Aylanc, S. Ertosun, A.F. Peixoto, A. Santamaria-Echart, P. Russo-Almeida, N. Vale, C. Freire, M. Vilas-Boas, Development of natural sporopollenin microcapsules: from bee pollen to versatile biomaterials, Emergent Mater (2025) 1–16, https://doi.org/10.1007/s42247-025-01002-1.

[21] M. Kieliszek, K. Piwowarek, A.M. Kot, S. Błażejak, A. Chlebowska-Śmigiel, I. Wolska, Pollen and bee bread as new health-oriented products: a review, Trends Food Sci. Technol. 71 (2018) 170–180, https://doi.org/10.1016/j.tifs.2017.10.021.

[22] J. Skopinska-Wisniewska, A. Sionkowska, A. Kaminska, A. Kaznica, R. Jachimiak, T. Drewa, Surface characterization of collagen/elastin based biomaterials for tissue regeneration, Appl. Surf. Sci. 255 (2009) 8286–8292, https://doi.org/10.1016/j.apsusc.2009.05.127.

[23] S.F.F.S. Yaacob, R.Z.R. Jamil, F.B.M. Suah, Sporopollenin based materials as a versatile choice for the detoxification of environmental pollutants — a review, Int. J. Biol. Macromol. 207 (2022) 990–1004, https://doi.org/10.1016/j.ijbiomac.2022.03.206.

[24] A. Bilgic, A. Cimen, A.N. Kursunlu, H.S. Karapınar, Novel fluorescent microcapsules based on sporopollenin for removal and detection of Cu (II) ions in aqueous solutions: eco-friendly design, fully characterized, photophysical&physicochemical data, Microporous Mesoporous Mater. 330 (2022) 111600, https://doi.org/10.1016/j.micromeso.2021.111600.

[25] D. Li, L. Sun, L. Shi, L. Zhuo, L. Yang, J. Zhang, Y. Han, T. Ye, S. Wang, Reversible switchable wettability of intrinsic micro/nanostructured pollen microcarriers via pH-induce from superhydrophobicity to superhydrophilicity, Chem. Eng. J. 473 (2023) 145184, https://doi.org/10.1016/j.cej.2023.145184.

[26] A. Sionkowska, The processes induced by UV light in biopolymers and biopolymer composites, Mol. Cryst. Liq. Cryst. 590 (2014) 17–23, https://doi.org/10.1080/15421406.2013.873624.

[27] P. Bhati, A. Srivastava, R. Ahuja, P. Chauhan, P. Vashisth, N. Bhatnagar, Physicochemical properties of UV-irradiated, biaxially oriented PLA tubular scaffolds, Polymers (basel) 15 (2023) 1097, https://doi.org/10.3390/polym15051097.

[28] H. Kaczmarek, J. Kowalonek, A. Szalla, A. Sionkowska, Surface modification of thin polymeric films by air-plasma or UV-irradiation, Surf. Sci. 507–510 (2002) 883–888, https://doi.org/10.1016/S0039-6028(02)01367-5.

[29] W. Brand-Williams, M.E. Cuvelier, C. Berset, Use of a free radical method to evaluate antioxidant activity, LWT Food Sci. Technol. 28 (1995) 25–30, https://doi.org/10.1016/S0023-6438(95)80008-5.

[30] T. Wang, E. Fleming, Y. Luo, An overview of the biochemistry, synthesis, modification, and evaluation of mucoadhesive polymeric nanoparticles for oral delivery of bioactive compounds, Adv. Compos. Hybrid Mater. 6 (2022) 1–19, https://doi.org/10.1007/s42114-022-00586-0.

[31] X. Wang, J. Chen, W. Jia, K. Huang, Y. Ma, Comparing the aging processes of PLA and PE: the impact of UV irradiation and water, Processes 12 (2024) 635, https://doi.org/10.3390/pr12040635.

[32] A. Lutzke, K.J. Morey, J.I. Medford, M.J. Kipper, Detailed characterization of Pinus ponderosa sporopollenin by infrared spectroscopy, Phytochemistry 170 (2020) 112195, https://doi.org/10.1016/j.phytochem.2019.112195.

[33] A. Mikhael, K. Jurcic, C. Schneider, D. Karr, G.L. Fisher, T.D. Fridgen, A. Diego-Taboada, P.E. Georghiou, G. Mackenzie, J. Banoub, Demystifying and unravelling the molecular structure of the biopolymer sporopollenin, Rapid Commun. Mass Spectrom. 34 (2020) e8740.

[34] W.T. Fraser, B.H. Lomax, P.E. Jardine, W.D. Gosling, M.A. Sephton, Pollen and spores as a passive monitor of ultraviolet radiation, Front. Ecol. Evol. 2 (2014) 86289, https://doi.org/10.3389/fevo.2014.00012.

[35] E.L. Tan, M.G. Potroz, G. Ferracci, L. Wang, J.A. Jackman, N.J. Cho, Hydrophobic to superhydrophilic tuning of multifunctional sporopollenin for microcapsule and bio-composite applications, Appl. Mater. Today 18 (2020) 100525, https://doi.org/10.1016/j.apmt.2019.100525.

[36] P.E. Jardine, F.A.J. Abernethy, B.H. Lomax, W.D. Gosling, W.T. Fraser, Shedding light on sporopollenin chemistry, with reference to UV reconstructions, Rev. Palaeobot. Palynol. 238 (2017) 1–6, https://doi.org/10.1016/j.revpalbo.2016.11.014.

[37] P.A.R. Fernandes, M.A. Coimbra, The antioxidant activity of polysaccharides: a structure-function relationship overview, Carbohydr. Polym. 314 (2023) 120965, https://doi.org/10.1016/j.carbpol.2023.120965.

[38] T. Fargere, M. Abdennadher, M. Delmas, B. Boutevin, Determination of peroxides and hydroperoxides with 2,2-diphenyl-1-picrylhydrazyl (DPPH). Application to ozonized ethylene vinyl acetate copolymers (EVA), Eur. Polym. J. 31 (1995) 489–497, https://doi.org/10.1016/0014-3057(94)00201-0.

[39] S. Anitha, S. Krishnan, K. Senthilkumar, V. Sasirekha, A comparative investigation on the scavenging of 2,2-diphenyl-1-picrylhydrazyl radical by the natural antioxidants (+) catechin and (−) epicatechin, J. Mol. Struct. 1242 (2021) 130805, https://doi.org/10.1016/j.molstruc.2021.130805.

[40] M.C. Foti, Use and Abuse of the DPPH• Radical, J. Agric. Food Chem. 63 (2015) 8765–8776, https://doi.org/10.1021/acs.jafc.5b03839.

[41] S.F. Souza, M. Mariano, D. Reis, C.B. Lombello, M. Ferreira, M. Sain, Cell interactions and cytotoxic studies of cellulose nanofibers from Curauá natural fibers, Carbohydr. Polym. 201 (2018) 87–95, https://doi.org/10.1016/j.carbpol.2018.08.056.

[42] B. Acharya, A. Behera, K. Deshmukh, S. Moharana, 4 - Biocompatibility, biodegradability, and toxicity evaluations of chitosan nanoparticles, in: K. Deshmukh, J. Mohan Dodda, I.M. El-Sherbiny, E.R. Sadiku (Eds.), Fundamentals and Biomedical Applications of Chitosan Nanoparticles, Woodhead Publishing, 2025, pp. 139–187, https://doi.org/10.1016/B978-0-443-14088-4.00007-1.

[43] S. Cai, C. Wu, W. Yang, W. Liang, H. Yu, L. Liu, Recent advance in surface modification for regulating cell adhesion and behaviors, Nanotechnol. Rev. 9 (2020) 971–989, https://doi.org/10.1515/ntrev-2020-0076.

[44] A. Ranella, M. Barberoglou, S. Bakogianni, C. Fotakis, E. Stratakis, Tuning cell adhesion by controlling the roughness and wettability of 3D micro/nano silicon structures, Acta Biomater. 6 (2010) 2711–2720, https://doi.org/10.1016/j.actbio.2010.01.016.